A Process-Oriented Framework for Understanding and Engineering Majorana Zero Modes: Insights from the Physical Interpretation of Ginzburg-Landau Parameters

Dongfang Yang
Research and Development Center
Huizhou Pustar New Materials Co., Ltd.
Huizhou 516267, China
Leo.yang@pustar.com

February 16, 2026

Abstract

The quest for robust and manipulable Majorana zero modes in topological superconductors faces multifaceted challenges, ranging from material realization to unambiguous experimental detection and quantum control. While the topological band theory provides a fundamental classification, it often lacks a phenomenological language to describe the processes that govern the stability and response of MZMs in real materials. This paper introduces a novel theoretical framework that bridges this gap by reinterpreting the phenomenological parameters of Ginzburg-Landau theory–α, β, and m^*–as three universal physical processes: energy competition, condensation saturation, and Cooper pair inertial mass. We establish that the stability of the topological superconducting phase hosting MZMs is governed by the delicate interplay and internal constraints among these processes. Specifically, we demonstrate that the energy competition α is rooted in quantum interference of matter waves, whose anisotropy is crucial for topological pairing. The saturation parameter β acts as a confining potential, defining the energy landscape for moving MZMs. The inertial mass m^*, enhanced by orbital angular momentum-local electric field coupling ($L \times E$ coupling), dictates the collective response and sets the adiabatic conditions for braiding. This framework offers a unified process-oriented perspective to dissect key unsolved puzzles in the MZM field: it explains the material fragility of topological superconductivity, provides an energy-scale picture for non-Abelian braiding, suggests new interpretations for local probe signals, and proposes parameter engineering especially via electric field control of m^* as a strategic path toward building MZM networks. Our work shifts the paradigm from merely describing topological properties to actively designing and manipulating the underlying physical processes that enable them.

Keywords: Majorana zero mode, topological superconductivity, Ginzburg-Landau theory, energy competition, condensation saturation, inertial mass, non-Abelian braiding, quantum computation.

1 Introduction

Majorana zero modes, exotic quasiparticle excitations predicted to emerge at the boundaries or defects of topological superconductors, have captivated condensed matter physics due to their non-Abelian exchange statistics and potential for fault-tolerant topological quantum computation [5, 6]. The seminal theoretical proposals for realizing MZMs in one-dimensional systems, such as spin-orbit-coupled semiconductor nanowires proximate to s-wave superconductors [13, 14], paved the way for these experimental endeavors. Significant experimental efforts have reported signatures consistent with MZMs in various platforms, including semiconductor nanowire-superconductor hybrids [7, 8], magnetic atom chains on superconductors [9], and iron-based superconductors [10, 15]. However, the field remains plagued by ambiguous evidence, material instability, and formidable challenges in achieving controlled manipulation [11, 12].

The core challenge lies in the transition from observing suggestive signatures to engineering and manipulating robust MZMs. While topological band theory elegantly classifies TSCs, its connection to the material-specific, dynamic processes that determine the stability and properties of MZMs is often indirect. A complementary, phenomenologically rich description is needed to bridge the microscopic quantum mechanics and the macroscopic experimental observations.

In this work, we propose such a bridge by adopting a novel interpretation of the classic Ginzburg-Landau theory of superconductivity [16]. Recent theoretical advances have reinterpreted the three phenomenological GL parameters–α, β, and m^*–not as mere fitting constants, but as direct manifestations of three fundamental physical processes: energy competition α between ordering and disordering energies, rooted in matter-wave interference; condensation saturation β representing the energetic cost of confining the condensate; and Cooper pair inertial mass m^* characterizing the collective inertia of the phase-coherent condensate, enhanced by orbital angular momentum-local electric field coupling ($L \times E$ coupling) in broken-inversion-symmetry environments [1, 2, 3]. These processes, governed by intrinsic scaling laws and mutual constraints, e.g., $-\alpha \propto m^*$ in strongly correlated systems, offer a unified framework to describe diverse superconducting families [4].

We apply this process-oriented GL framework to the physics of MZMs. Our central thesis is that the existence, stability, and manipulability of an MZM are not solely determined by topological invariants but are profoundly influenced by the local and global balance of these three GL processes in the host superconductor. This perspective yields fresh insights into persistent puzzles:

- **Material Design:** The scarcity of robust, high-temperature TSCs is linked to the stringent requirement for anisotropic matter-wave interference for topological α coexisting with strong $L \times E$ environments affecting m^*, which are often mutually disruptive.
- **Braiding Dynamics:** The adiabatic condition for non-Abelian braiding is shown to be governed by an energy landscape set by β and a kinematic response governed by m^*.
- **Experimental Signatures:** Local probes like scanning tunneling microscopy can perturb the local m^* via tip-induced electric fields, complicating the interpretation of zero-bias peaks.
- **Network Engineering:** The coupling between MZMs in a network is parameterized by GL quantities n_s, α, β, m^*, suggesting that electric field control of m^* via the $L \times E$ mechanism could be a potent tool for tuning coupling strengths.

This paper is structured as follows. In Section 2, we review the process-oriented GL theory and its microscopic underpinnings. Section 3 applies this framework to analyze the stability conditions for TSCs hosting MZMs. Section 4 discusses implications for experimental observation and characterization. Section 5 explores the braiding and manipulation of MZMs through the lens of GL processes. Section 6 considers the engineering of MZM networks via parameter control. We conclude in Section 7 with a summary and outlook.

2 The Process-Oriented Ginzburg-Landau Framework

The standard GL free energy density for a superconductor is [16]

$$f_{\mathrm{GL}} = \alpha|\psi|^2 + \frac{\beta}{2}|\psi|^4 + \frac{1}{2m^*}|(-i\hbar\nabla - 2e\mathbf{A})\psi|^2 + \frac{B^2}{2\mu_0}, \tag{1}$$

where ψ is the complex order parameter, and $\alpha = \alpha_0(T - T_c)$ near T_c. Conventionally, α, β, and m^* are treated as phenomenological constants. Recent work reinterprets them as scales for three core processes.

2.1 Energy Competition α: Matter-Wave Interference and Pairing

The parameter α is defined as the difference between disordering and ordering energy, $\alpha = U_{\mathrm{dis}} - U_{\mathrm{ord}}$. It becomes negative below T_c, driving the phase transition. Microscopically, a negative α (net attraction) arises from a redistribution of interaction energies due to constructive matter-wave interference at specific wavevectors [2]. This microscopic basis connects the phenomenological GL theory to the fundamental BCS pairing mechanism [17] and its rigorous derivation by Gor'kov [18]. For conventional s-wave pairing, this interference is isotropic. For topological (e.g., p-wave) pairing, the interference pattern must be anisotropic and possess a specific momentum-space structure (e.g., odd parity) to generate spin-triplet or mixed-parity pairing. This immediately highlights the fragility of topological α: disorder, multi-band effects, or symmetry-breaking fields can easily disrupt the delicate interference condition.

2.2 Condensation Saturation β: The Confinement Potential

The $\beta|\psi|^4$ term prevents unlimited growth of $|\psi|^2$. It is interpreted as the energy cost of confining the charged, massive Cooper pair condensate within a coherence volume ξ^3, analogous to a centrifugal pressure [3]. A mechanical analogy arises: β corresponds to an effective centrifugal pressure resisting confinement. The equilibrium order parameter $|\psi|^2 = -\alpha/\beta$ represents a balance between the inward condensation pressure $-\alpha$ and this outward centrifugal pressure $\beta|\psi|^2$. Thus, β defines a stiffness against spatial variations of $|\psi|$.

2.3 Cooper Pair Inertial Mass m^*: Collective Inertia and $L \times E$ Coupling

The parameter m^* is not the bare mass of a Cooper pair but the inertial mass of the phase-coherent condensate as a whole, governing its response to phase gradients (supercurrent) and time-dependent perturbations. It determines the phase stiffness $\rho_s = n_s/m^*$ with n_s the superfluid density. In systems with broken inversion symmetry or strong local electric fields $\mathbf{E}$, the coupling between orbital angular momentum $\mathbf{L}$ and $\mathbf{E}$ ($L \times E$ coupling) significantly enhances m^* [4]. This occurs through both single-particle band renormalization and additional scattering channels for collective phase dynamics. The enhancement follows a scaling law $m^* \propto \lambda_{L\times E}^2$, where $\lambda_{L\times E}$ characterizes the coupling strength.

$$m^* = m_0^* \left(1 + \eta \frac{\lambda_{L\times E}^2 E_{\text{loc}}^2}{\Delta_{\text{band}}^2}\right), \tag{2}$$

where m_0^* is the band mass, η a material constant, E_{loc} the local electric field, and Δ_{band} a characteristic band splitting.

2.4 Internal Constraints and Scaling Laws

These processes are not independent. Theoretical self-consistency, as derived from microscopic foundations linking GL theory to pairing interactions, imposes internal constraints among them [1]. A key constraint in strongly correlated systems is

$$-\alpha \propto m^*, \quad \beta \propto m^*. \tag{3}$$

This implies that mechanisms enhancing pairing ($-\alpha$) often concomitantly increase inertial mass m^*. The superconducting transition temperature scales as $T_c \propto \sqrt{-\alpha/m^*} \equiv \sqrt{K}$, where K is the specific pairing efficiency. High T_c requires optimizing K, not just maximizing $-\alpha$.

3 Stability of Topological Superconducting Phases Hosting MZMs

A topological superconducting phase requires a bulk pairing gap with non-trivial topological invariants, leading to boundary MZMs. Using the GL process framework, we analyze the conditions for such a phase to be stable.

3.1 Topological Pairing and the Anisotropy of α

For a time-reversal-invariant p-wave or similar topological pairing, the order parameter has a vector or matrix structure $\vec{\psi}$ (e.g., d-vector). The GL expansion becomes more complex, but the core process α now pertains to the anisotropic interference condition. In momentum space, the pairing interaction $V_{\mathbf{k},\mathbf{k}'}$ must have a sign change (e.g., $V \sim \cos\theta$ for p_x-wave). This corresponds to a highly directional matter-wave interference pattern. The GL parameter α for each component ψ_i is then sensitive to crystal orientation, strain, and disorder, which can average out the anisotropy, driving the system towards a topologically trivial state (e.g., s-wave). Thus, material platforms that preserve and isolate the required anisotropic interference are rare.

3.2 Role of β and m^* in Gap Stability

The bulk superconducting gap $\Delta \propto \sqrt{-\alpha/\beta}$. For a TSC, a large Δ is desirable to protect MZMs from thermal excitations. Equation 3 suggests that in strongly correlated candidates (e.g., certain iron-based superconductors), attempts to increase Δ by enhancing $-\alpha$ may also increase m^* and β, potentially saturating Δ. Moreover, a large m^* (high inertia) implies a low phase stiffness ρ_s, making the superconductor

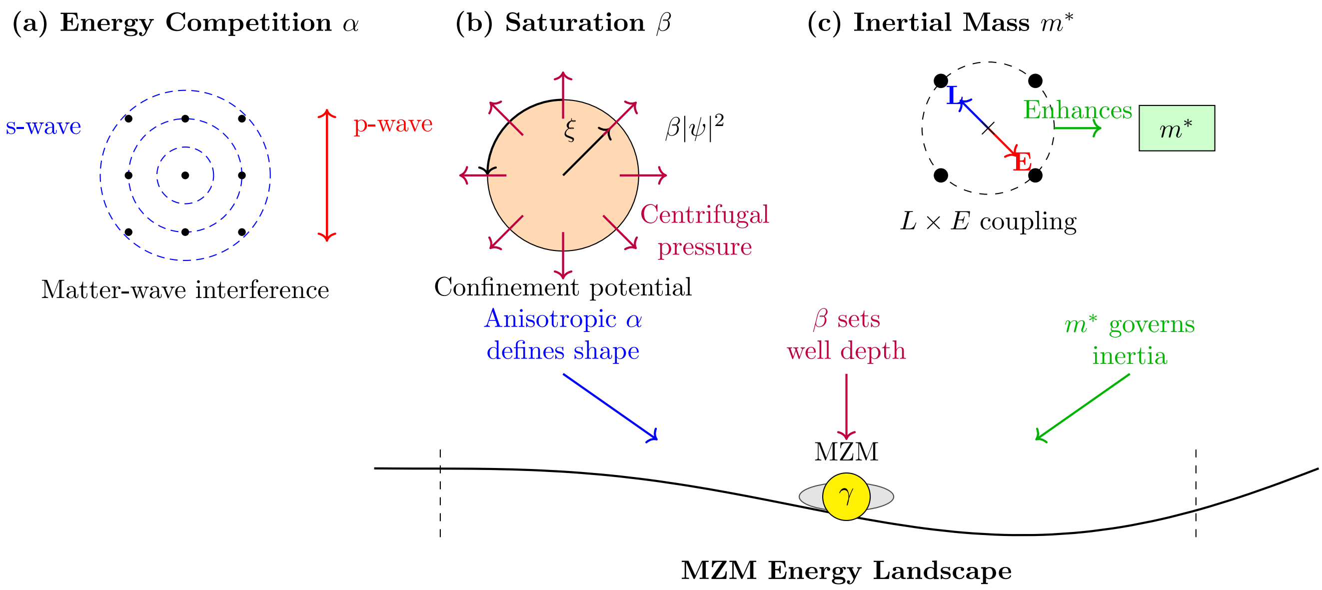

Figure 1: Schematic of the process-oriented GL framework governing the MZM energy landscape. (a) Energy competition α: s-wave (isotropic, blue) vs. p-wave (anisotropic, red) matter-wave interference patterns. (b) Condensation saturation β: acts as a centrifugal pressure (purple arrows) confining the condensate within a coherence volume ξ, creating a local suppression (orange). (c) Inertial mass m^*: enhanced by the $L \times E$ coupling in broken-symmetry environments. Bottom: The combined effect defines an energy landscape where the MZM (γ) resides in a potential well shaped by α, β, and m^*.

more susceptible to phase fluctuations that can destroy long-range order, particularly in low-dimensional systems (e.g., nanowires, chains). This trade-off is critical for low-dimensional TSC candidates.

3.3 Consequences of Inversion Symmetry Breaking: $L \times E$ Coupling and Mass Enhancement

Many proposed TSC platforms (e.g., heterostructures, thin films, nanowires) inherently lack inversion symmetry, activating the $L \times E$ coupling. As derived in [4], this coupling enhances m^* by

$$m^* = m_0^* \left(1 + \eta \frac{\lambda_{L\times E}^2 E_{\text{loc}}^2}{\Delta_{\text{band}}^2}\right). \tag{4}$$

Enhanced m^* reduces ρ_s and T_c since $T_c \propto 1/\sqrt{m^*}$ for fixed α. Therefore, strong interfacial fields (needed for Rashba spin-orbit coupling crucial for many TSC proposals) come at the cost of increased m^*, which may suppress superconductivity unless pairing ($-\alpha$) is simultaneously enhanced by the same fields (a possibility via the inverse Edelstein effect). This delicate balance explains the narrow parameter windows observed in many synthetic TSCs. Conceptually, this can be visualized in a two-dimensional phase space spanned by the pairing strength '$-\alpha$' and the '$L \times E$' coupling strength '$\lambda_{L\times E}E$'. The topological superconducting phase likely occupies a slender region where '$-\alpha$' is sufficiently large and anisotropic to support topological pairing, while '$\lambda_{L\times E}E$' is within an intermediate range—too weak to induce sufficient Rashba spin-orbit coupling for creating MZMs, yet too strong leading to a heavily enhanced 'm^*' that suppresses 'T_c' and phase coherence.

4 Implications for Experimental Observation

Experimental detection of MZMs relies heavily on local probes like scanning tunneling microscopy, which measure the local density of states.

4.1 LDOS at an MZM and GL Parameters

Within a simplified Bogoliubov-de Gennes model, an MZM at position $\mathbf{r}_0$ contributes a delta-function peak at zero energy in the LDOS. In reality, the peak is broadened by lifetime effects and instrumental resolution. More subtly, the local environment of the MZM, described by spatially varying GL parameters, shapes the peak. If the MZM is located at a vortex core or wire end, the order parameter $|\psi(\mathbf{r})|$ vanishes at $\mathbf{r}_0$ and recovers over ξ. The local gap $\Delta(\mathbf{r}) \propto |\psi(\mathbf{r})|$ is thus suppressed. The spatial profile of $|\psi|$ is determined by the GL equations involving $\alpha(\mathbf{r}), \beta(\mathbf{r})$, and $m^*(\mathbf{r})$. Inhomogeneities (defects, strain) can cause spatial variations in these parameters, leading to a disorder-broadened MZM wavefunction and a widened ZBP. To elaborate, consider spatial fluctuations in '$\alpha(\mathbf{r})$' and '$m^*(\mathbf{r})$' due to defects, characterized by a correlation length 'l_{dis}'. The MZM wavefunction localization is governed not only by the coherence length 'ξ' but also by 'l_{dis}' and the correlation between fluctuations in 'α' and 'm^*'. If the constraint '$-\alpha \propto m^*$' holds strongly locally, their ratio '$K(\mathbf{r}) = -\alpha(\mathbf{r})/m^*(\mathbf{r})$' remains relatively constant spatially. This spatial uniformity of 'K' can lead to a more stable MZM energy compared to cases where 'α' and 'm^*' fluctuate independently.

4.2 STM Tip-Induced Perturbation of m^*

An STM tip generates a strong, localized electric field $\mathbf{E}_{\text{tip}}$. According to the $L \times E$ mechanism (Eq. 2), this field modifies the local m^* beneath the tip. When the tip is positioned over a suspected MZM, the changed inertia alters the local phase dynamics and may shift the energy of the MZM or distort its wavefunction. This effect depends on tip voltage, distance, and the material's $\lambda_{L\times E}$. It provides a potential microscopic mechanism for tip-induced gating of ZBPs observed in some experiments [10]. Distinguishing this effect from trivial bound states requires monitoring the ZBP evolution with tip conditions—a testable prediction of our framework. A concrete experimental protocol would involve systematically varying the STM tip height (to modulate the perturbing field 'δE') and/or bias voltage (which may affect the local 'E_{loc}'), while precisely tracking the resulting shift in the ZBP energy 'δE_0'. A reproducible, quantitative relationship between 'δE_0' and the tip parameters that aligns with the expected '$\delta m^* \propto E_{\text{loc}} \cdot \delta E$' dependence from the '$L \times E$' mechanism could provide compelling evidence for the Majorana nature of the state, beyond signatures from trivial Andreev bound states.

4.3 Interpreting "Zero Energy" within the Constraint

The constraint $-\alpha \propto m^*$ implies that local fluctuations in pairing strength are tied to fluctuations in inertia. A region with stronger pairing (more negative α) likely also has a larger m^*. The MZM energy E_0 is determined by the overlap of wavefunctions across such fluctuations. Since both α and m^* scale together, their ratio $K = -\alpha/m^*$ may be more spatially uniform than either alone, promoting a more robust zero energy. This offers a new criterion for MZM robustness: materials with strong internal constraints may host MZMs less sensitive to disorder.

5 Braiding Dynamics from an Energy Landscape Perspective

Braiding MZMs requires adiabatically moving them along specified paths. Our framework provides an energy-scale description of this process.

5.1 The Confining Potential $\beta|\psi|^2$ and MZM Mobility

An MZM is pinned to a location where the order parameter vanishes (e.g., vortex core). To move it, one must deform the $|\psi|$ landscape, which costs energy proportional to $\beta \int (\delta|\psi|^2)^2 dV$. The parameter β thus acts as a confining potential (stiffness). For a vortex in a type-II superconductor, the force needed to move it is related to the pinning potential, which scales with $\beta H_c^2 \xi^3$ (H_c is the thermodynamic critical field). A large β implies a deep pinning potential, making MZMs harder to move but also less susceptible to accidental displacement by noise. This trade-off informs braiding speed and error rates.

5.2 Adiabatic Condition and Inertial Mass m^*

The adiabatic theorem requires the braiding timescale τ to be much longer than the inverse of the minimum excitation gap $\Delta_{\min}$ along the path: $\tau \gg \hbar/\Delta_{\min}$. However, $\Delta_{\min}$ itself is affected by the motion. As an MZM moves, it perturbs the phase field $\phi(\mathbf{r}, t)$. The dynamics of ϕ are governed by an effective wave equation with a "mass" term related to m^* [1]. A large m^* slows down the phase relaxation, meaning that after moving an MZM, the system takes longer to settle into its new ground state. Therefore, the adiabatic condition must also satisfy $\tau \gg \tau_{\text{relax}}$, where the phase relaxation time scale τ_{relax} can be estimated from the phase stiffness ρ_s and the inertial mass m^*. Considering the phase dynamics as a diffusive or propagating mode, one finds $\tau_{\text{relax}} \sim L^2 m^*/\rho_s$ for an overdamped response or $\tau_{\text{relax}} \sim L\sqrt{m^*/\rho_s}$ for an underdamped response, with L being the system size. This additional constraint can be stringent in materials with large m^* (e.g., heavy-fermion or strongly spin-orbit-coupled systems).

5.3 Energetics of Braiding Operations

Consider two MZMs, γ_1 and γ_2, separated by distance L. Their coupling energy $E_{\text{coup}} \sim \Delta e^{-L/\xi}$ depends on $\xi = \hbar/\sqrt{m^*|\alpha|}$. Braiding involves changing L in time. The work done against the confining potential (related to β) and the kinetic energy associated with phase dynamics (related to m^*) must be supplied externally and dissipated as heat. Minimizing non-adiabatic excitations requires slow, controlled trajectories—a challenge quantified by the GL parameters.

6 Towards MZM Networks: Parameter Engineering

Building a topological quantum computer requires a network of coupled MZMs with tunable couplings.

6.1 Coupling Strength as a Function of GL Parameters

The Josephson coupling energy E_J between two superconducting islands hosting MZMs can be derived from the Ginzburg-Landau formalism. For a weak link with cross-sectional area A (treated as constant), the coupling scales as $E_J \sim (n_s/m^*)A\Delta$, stemming from the standard GL current-phase relation. This aligns with the Ambegaokar-Baratoff intuition where E_J is related to the product of the gap Δ and the normal-state conductance. Substituting the equilibrium GL relations $n_s \propto |\psi|^2 = -\alpha/\beta$ and $\Delta \propto \sqrt{-\alpha/\beta}$, we arrive at

$$E_J \propto \frac{(-\alpha)^{3/2}}{m^* \beta^{1/2}}. \tag{5}$$

Given the constraints 3, in correlated systems $E_J \propto (-\alpha)^{1/2} \propto m^{*1/2}$. Thus, coupling strength increases with pairing strength and inertial mass, albeit sublinearly. This suggests that stronger pairing materials (larger $-\alpha$) offer stronger inter-MZM coupling, beneficial for gate operations.

6.2 Electric Field Control via $L \times E$ Coupling

Equation 2 indicates that m^* can be tuned by a local electric field E_{loc}. Placing a gate electrode near an MZM or a junction allows one to modulate m^*, and hence E_J via 5. This provides a non-magnetic, potentially fast control knob for tuning coupling between MZMs. Since the $L \times E$ coupling is sensitive to crystal orientation, anisotropic control may be possible. Such electric-field control aligns with the desire to minimize magnetic fields that could disturb superconductivity. As a concrete design example, consider two topological superconducting islands connected by a narrow Josephson junction. A gate electrode placed above the junction region modulates the local electric field 'E_{loc}', thereby tuning the junction's 'm^*' via Eq. (2). Assuming other parameters ('α', 'β', 'n_s') in the junction remain approximately constant under gating, the Josephson coupling 'E_J' scales as '$E_J \propto 1/m^*$' (from Eq. (5)). The coupling tunability, defined as '$\partial E_J/\partial V_g$', then depends on material-specific factors like '$\lambda_{L\times E}$' and 'η', and the gate geometry determining '$\partial E_{\text{loc}}/\partial V_g$'. Achieving a large on/off ratio (e.g., > 10) for the coupling requires materials with a strong '$L \times E$' response and optimized gate design to maximize field penetration.

6.3 Designing Parameter Landscapes

A network of MZMs can be envisioned as a lattice of regions with engineered GL parameters. For instance, one could create "islands" with high $-\alpha$ (strong pairing) connected by "links" with lower β (easier to modulate coupling). The $L \times E$ mechanism allows electric fields to reconfigure these landscapes dynamically. Challenges include cross-talk between gates and ensuring that field-induced changes in m^* do not inadvertently suppress α (pairing). Materials with strong intrinsic constraints 3 may mitigate this by keeping $K = -\alpha/m^*$ relatively constant under gating. For "island" regions meant to stably host MZMs, the target parameter profile is: large '$-\alpha$' (strong pairing), moderate 'm^*' (to avoid suppressing 'T_c' and phase stiffness), and large 'β' (deep pinning potential to localize MZMs). In contrast, "link" regions for tunable coupling require: moderate '$-\alpha$' (maintaining superconductivity), highly tunable 'm^*' (via strong '$L\times E$' coupling susceptibility for efficient gating), and relatively small 'β' (lower energy cost to modulate the order parameter for coupling control). Material growth or nano-fabrication techniques that can spatially pattern such parameter landscapes pose a significant challenge. Furthermore, capacitive cross-talk between adjacent gates can smear the intended '$E_{\rm loc}$' profile, limiting control fidelity. The speed limit for electric field tuning of 'm^*' and 'E_J', governed by the electronic response and scattering channels underlying the '$L \times E$' mechanism, is estimated to be in the picosecond to nanosecond range, which is compatible with envisioned quantum gate operation speeds.

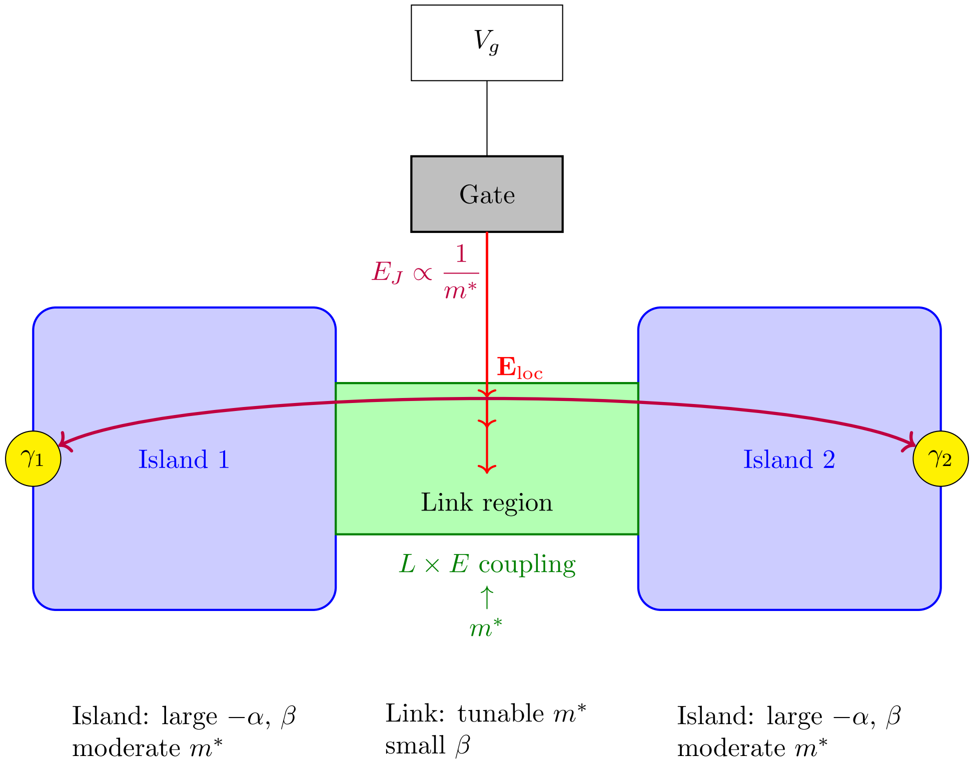

Figure 2: Electric-field control of Majorana coupling via the $L \times E$ mechanism. Two topological superconducting "islands" (blue), each hosting an MZM (γ_1, γ_2), are connected by a "link" region (green). A gate electrode above the link applies a voltage V_g, creating a local electric field $\mathbf{E}_{\rm loc}$. This field, via the $L \times E$ coupling, modulates the inertial mass m^* in the link. Since the Josephson coupling energy E_J between the islands scales inversely with m^*, the gate voltage provides direct control over the MZM coupling strength, enabling the formation of tunable networks.

7 Conclusion and Outlook

We have introduced a novel process-oriented framework, based on the physical interpretation of Ginzburg-Landau parameters, to analyze the challenges and opportunities in the field of Majorana zero modes. By recasting the GL parameters α, β, and m^* as manifestations of fundamental processes—energy competition rooted in matter-wave interference, condensation saturation (confinement potential), and Cooper pair inertial mass enhanced by $L \times E$ coupling—we provide a unified phenomenological language that bridges microscopic quantum mechanics and macroscopic material properties.

This framework sheds new light on key unsolved problems:

- The scarcity of robust topological superconductors is understood as a consequence of the delicate anisotropic interference required for topological pairing, often disrupted by the same strong spin-orbit and $L \times E$ environments needed for MZMs.

- The braiding of MZMs is framed as an adiabatic navigation of an energy landscape shaped by β, with speed limits set by the inertial mass m^*.
- Experimental signatures, like STM zero-bias peaks, must be interpreted considering tip-induced perturbations to the local m^*.
- The engineering of MZM networks can be approached as a problem of spatially patterning and dynamically controlling the GL parameters, with electric field gating of m^* via the $L\times E$ mechanism offering a promising control strategy.

As an extension of this framework, the process-oriented energetics perspective provides a complementary angle for analyzing topological superconducting systems. By leveraging the interplay and constraints among α, β, and the effective mass m^*, one can characterize the dynamical features of the topological superconducting condensation process from the viewpoint of energy evolution. This complements existing descriptions based on momentum-space pairing symmetry and real-space topological order, with a sharper focus on the universal physics governing the condensation process itself.

Building upon the proposed framework, future theoretical efforts should prioritize the development of quantitative models capable of incorporating the spatiotemporal variations of α, β, and m^* within realistic device geometries. Subsequent calculations of observable quantities, such as the local density of states and Josephson currents, within this framework are essential. On the experimental front, systematically investigating the influence of electric fields, strain, and disorder on the superconducting properties of candidate materials from the perspective of Ginzburg-Landau processes can offer valuable guidance for material optimization. Ultimately, the realization of fault-tolerant topological quantum computing requires not only harnessing the topologically protected nature of Majorana zero modes but also deeply understanding and engineering the classical physical processes governing their material environment. The framework presented in this work provides a conceptual roadmap for achieving such precise control.

Funding

This research received no external funding.

Institutional Review Board Statement

Not applicable.

Informed Consent Statement

Not applicable.

Data Availability Statement

Data sharing is not applicable to this article as no datasets were generated or analyzed during the current study.

Acknowledgments

The author acknowledges the supportive research environment at the Research and Development Center of Huizhou Pustar New Materials Co., Ltd.

Conflicts of Interest

The author declares no conflicts of interest.

References

[1] Yang, D. Physical Processes Underlying Ginzburg-Landau Theory: Energy Competition, Condensation Saturation, and Cooper Pair Inertial Mass Scaling Laws. *NextGen Physics* **2026**.

[2] Yang, D. Microscopic Origin of Superconducting Energy Competition: Matter Wave Interference and Energy Redistribution. *NextGen Physics* **2026**.

[3] Yang, D. A Geometrodynamic Interpretation of the β-Parameter in Ginzburg-Landau Theory: Centrifugal Saturation of the Superconducting Condensate. *NextGen Physics* **2026**.

[4] Yang, D. Enhancement Mechanism of Cooper Pair Inertial Mass: Orbital Angular Momentum-Local Field $L \times E$ Coupling. *NextGen Physics* **2026**.

[5] Kitaev, A. Yu. Fault-tolerant quantum computation by anyons. *Ann. Phys.* **2003**, *303*(1), 2–30.

[6] Nayak, C.; Simon, S.H.; Stern, A.; Freedman, M.; Das Sarma, S. Non-Abelian anyons and topological quantum computation. *Rev. Mod. Phys.* **2008**, *80*, 1083–1159.

[7] Mourik, V.; Zuo, K.; Frolov, S.M.; Plissard, S.R.; Bakkers, E.P.A.M.; Kouwenhoven, L.P. Signatures of Majorana Fermions in Hybrid Superconductor-Semiconductor Nanowire Devices. *Science* **2012**, *336*(6084), 1003–1007.

[8] Deng, M.T.; Vaitiekenas, S.; Hansen, E.B.; Danon, J.; Leijnse, M.; Flensberg, K.; Nygard, J.; Krogstrup, P.; Marcus, C.M. Majorana bound state in a coupled quantum-dot hybrid-nanowire system. *Science* **2016**, *354*(6319), 1557–1562.

[9] Nadj-Perge, S.; Drozdov, I.K.; Li, J.; Chen, H.; Jeon, S.; Seo, J.; MacDonald, A.H.; Bernevig, B.A.; Yazdani, A. Observation of Majorana fermions in ferromagnetic atomic chains on a superconductor. *Science* **2014**, *346*(6209), 602–607.

[10] Sun, H. H.; Wang, D.; Zhu, S.; Fan, P.; Wen, C.; Mao, J.; Zhu, C.; Ma, H.; Wang, J.; Yang, Y.; et al. Majorana zero mode detected with spin selective Andreev reflection in the vortex of a topological superconductor. *Phys. Rev. Lett.* **2016**, *116*, 257003.

[11] Sarma, S. D.; Freedman, M.; Nayak, C. Majorana zero modes and topological quantum computation. *npj Quantum Inf.* **2015**, *1*, 15001.

[12] Lutchyn, R. M.; Bakkers, E. P. A. M.; Kouwenhoven, L. P.; Krogstrup, P.; Marcus, C. M.; Oreg, Y. Majorana zero modes in superconductor–semiconductor heterostructures. *Nat. Rev. Mater.* **2018**, *3*, 52–68.

[13] Oreg, Y.; Refael, G.; von Oppen, F. Helical Liquids and Majorana Bound States in Quantum Wires. *Phys. Rev. Lett.* **2010**, *105*, 177002.

[14] Lutchyn, R. M.; Sau, J. D.; Sarma, S. D. Majorana Fermions and a Topological Phase Transition in Semiconductor-Superconductor Heterostructures. *Phys. Rev. Lett.* **2010**, *105*, 077001.

[15] Sato, M.; Ando, Y. Topological superconductors: a review. *Rep. Prog. Phys.* **2017**, *80*, 076501.

[16] Ginzburg, V.L.; Landau, L.D. On the theory of superconductivity. *Zh. Eksp. Teor. Fiz.* **1950**, *20*, 1064–1082.

[17] Bardeen, J.; Cooper, L.N.; Schrieffer, J.R. Theory of superconductivity. *Phys. Rev.* **1957**, *108*, 1175–1204.

[18] Gor'kov, L.P. Microscopic derivation of the Ginzburg-Landau equations in the theory of superconductivity. *Sov. Phys. JETP* **1959**, *9*, 1364–1367.